

Consistent and Scalable Bayesian Joint Variable and Graph Selection for Disease Diagnosis Leveraging Functional Brain Network*

Xuan Cao[†] and Kyoungjae Lee^{‡,§}

Abstract. We consider the joint inference of regression coefficients and the inverse covariance matrix for covariates in high-dimensional probit regression, where the predictors are both relevant to the binary response and functionally related to one another. A hierarchical model with spike and slab priors over regression coefficients and the elements in the inverse covariance matrix is employed to simultaneously perform variable and graph selection. We establish joint selection consistency for both the variable and the underlying graph when the dimension of predictors is allowed to grow much larger than the sample size, which is the first theoretical result in the Bayesian literature. A scalable Gibbs sampler is derived that performs better in high-dimensional simulation studies compared with other state-of-art methods. We illustrate the practical impact and utilities of the proposed method via a functional MRI dataset, where both the regions of interest with altered functional activities and the underlying functional brain network are inferred and integrated together for stratifying disease risk.

Keywords: joint selection consistency, Markov random field prior, Parkinson's disease.

MSC2020 subject classifications: Primary 62F15, 62J12; secondary 62F12.

1 Introduction

Analyzing high-dimensional data is becoming increasingly prevalent and challenging as technology advances facilitating the collection and storage of more extensive massive data. When applying a generalized linear model (GLM) to such large-scale data, a large number of variables can easily cause an overfitting problem. In this situation, variable selection is one of the most commonly used techniques to avoid overfitting. Numerous frequentist methods on variable selection have been introduced ever since the appearance of Lasso (Tibshirani, 1996), and many analogous Bayesian methods have also been proposed (Ishwaran et al., 2005; Narisetty and He, 2014; Ročková and George, 2018).

*This work was supported in part by the Simons Foundation's collaboration grant (No.635213). Kyoungjae Lee was supported by the National Research Foundation of Korea (NRF) grant funded by the Korea government (MSIT) (No. 2020R1A4A1018207).

[†]Department of Mathematical Sciences, University of Cincinnati, Cincinnati, Ohio, USA, caox4@ucmail.uc.edu

[‡]Department of Statistics, Sungkyunkwan University, Seoul, South Korea, leekjstat@gmail.com

[§]Corresponding author.

On the other hand, understanding the complex relationships between variables in high-dimensional datasets is also important, where inverse covariance matrices (or equivalently, precision matrices) are prevalently exploited to capture the multivariate dependence. This is often called a network structure between the variables. A variety of work on algorithms and their theoretical considerations have emerged to investigate a network structure (Wainwright, 2019). One of key developments was the introduction of the neighborhood selection method (Meinshausen and Bühlmann, 2006), which leverages the connection between the (i, j) th entry of the inverse covariance matrix Ω to the partial correlation between the i th and j th variable estimated through a penalized regression setup. Many other frequentist methods have been developed for sparse precision matrix estimation based on the neighborhood selection (Yuan and Lin, 2007; Friedman et al., 2007; Peng et al., 2009; Khare et al., 2015), and several Bayesian counterparts have been proposed in the literature (Dobra et al., 2011; Wang, 2012, 2015). However, a key challenge for these Bayesian approaches is their scalability to high-dimensional settings. To address this issue, recently, Jalali et al. (2020) employed the regression-based generalized likelihood function in Khare et al. (2015) combined the spike and slab priors over entries in Ω . They proposed a scalable Gibbs sampler that works well in high dimensions and runs comparably fast compared with the Graphical Lasso (Friedman et al., 2007).

It is often of interest to jointly perform variable selection and discover the network structure among predictors. This type of problems is of wide clinical applications in radiological and genomic studies. Magnetic resonance imaging (MRI) scans and genetic traits are typical examples where the mechanism for effect on an outcome, such as functional brain activities (Langer et al., 2012) or molecular phenotypes such as gene expression, proteomics, or metabolomics (Nacu et al., 2007; Souza et al., 2020), often displays a coordinated change along a pathway. In such cases, the impact of a single factor may not be apparent. Specifically for radiological studies, recent progress in imaging analysis allows the development of a novel feature extraction method called radiomics which converts large amounts of medical imaging characteristics into high-dimensional mineable data pool to build a predictive and descriptive model. The method has been applied to the diagnosis of neuropsychiatric diseases such as autism, schizophrenia, and Alzheimer disease (Feng et al., 2019; Salvatore et al., 2021). These findings demonstrate the validity of these radiomic approaches in discovering discriminative features that can reveal pathological information. In such cases, the method of joint selection can incorporate and highlight the underlying brain network to improve the classification accuracy.

Several frequentist and Bayesian methods have been proposed for joint inference on variables and graphs. Li and Li (2008, 2010) investigated a graph-constrained regularization procedure as well as its theoretical properties in order to account for the neighborhood information of variables measured on a given graph. Dobra (2009) estimated a network among relevant predictors by first performing a stochastic search to discover subsets of predictors, then using a Bayesian model averaging approach to estimate a dependency network. Liu et al. (2014) developed a Bayesian method for regularized regression, which provides inference on the inter-relationship between variables

by explicitly modeling through a graph Laplacian matrix. Peterson et al. (2016) simultaneously inferred a sparse network among the predictors based on the block Gibbs sampler and performed variable selection using this network as guidance by incorporating it into a Markov random field (MRF) prior.

Despite recent advances in Bayesian methods for joint regression and covariance estimation, theory related to joint selection consistency is not well-understood. Some early attempts (Cao and Lee, 2021) focused solely on linear regression models, where the predictors are linked through a directed graph with a known ordering. To the best of our knowledge, joint variable and graph selection consistency in a high-dimensional GLM has not been investigated under either directed or undirected graphical models.

In this paper, we consider a high-dimensional probit model with network-structured predictors via a Gaussian graphical model. Our goal is to jointly perform variable and graph selection with theoretical guarantees, and to develop a scalable algorithm for joint inference in a high-dimensional regime. We fill the gap in the literature by establishing joint selection consistency of the proposed posterior distribution, which guarantees that the posterior probability assigned to the significant variables and the true graph tends to 1 as we observe more data. To perform joint selection, spike and slab priors, imposed on the regression coefficients and the precision matrix of predictors, are linked by an MRF prior. Furthermore, for scalable inference, we adopt the regression-based generalized likelihood function (Khare et al., 2015) for the predictors. This enables the derivation of a scalable Gibbs sampler by making available the conditional posteriors for the entries of the precision matrix in closed form. We illustrate the practical impact and utilities of the proposed method via a functional MRI dataset, where both the regions of interest with altered functional activities and the underlying functional brain network are inferred and integrated together for disease diagnosis.

We note here that we model the network among the covariates as an undirected graphical model. Alternatively, the network can also be modeled using a directed acyclic graph model, as was done in Chekouo et al. (2015), Peluso and Consonni (2020) and Cao and Lee (2021). Furthermore, we use the term “joint variable and graph selection” in a slightly different context from the meaning used in the existing multivariate regression literature. For examples, in Bhadra and Mallick (2013), Chen et al. (2016), Consonni et al. (2017), Deshpande et al. (2019) and Samanta et al. (2022), they considered multivariate regression models, where joint sparsity is imposed in the regression coefficient matrix and the error covariance matrix.

The rest of the paper is organized as follows. In Section 2, we describe the generalized likelihood function for inverse covariance estimation and the spike and slab priors for sparsity recovery under a probit regression. Posterior computation algorithms are described in Section 3. Theoretical results of the proposed posterior including joint variable and graph selection consistency are shown in Section 4 with proofs provided in the supplementary material (Cao and Lee, 2023). We show the performance of the proposed method and compare it with other competitors through simulation studies in Section 5. In Section 6, a radiomic analysis is conducted for predicting Parkinson’s disease based on functional MRI (fMRI) data, and a discussion is given in Section 7.

2 Model Specification

Consider a case-control study to identify the radiomic features that are network-structured and may contribute to the disease risk by comparing patients who have certain disease (the “cases”) with subjects who do not have that disease but are otherwise similar (the “controls”). In particular, for $i = 1, 2, \dots, n$, let $Y_i \in \{0, 1\}$ be the binary response variable indicating whether the i th subject has certain disease, and denote $X_i = (x_{i1}, x_{i2}, \dots, x_{ip})^T \in \mathbb{R}^p$ as the covariate vector containing all the p radiomic features for the i th subject. We consider the following probit model with covariates that obey a multivariate Gaussian distribution: for $1 \leq i \leq n$,

$$P(Y_i = 1 \mid X_i, \beta) = \Phi(X_i^T \beta), \quad (2.1)$$

$$X_i \mid \Omega \stackrel{i.i.d.}{\sim} N_p(0, \Omega^{-1}), \quad (2.2)$$

where $\Phi(\cdot)$ is the cumulative distribution function of the standard normal distribution, β is a $p \times 1$ vector of regression coefficients, and $\Omega = (\omega_{jk})$ denotes the $p \times p$ inverse covariance matrix. Our goal is to infer the regression coefficients β and underlying network structure Ω simultaneously to identify all the significant features better.

2.1 CONCORD Generalized Likelihood for Predictors

In the frequentist setting, one of the most popular methods to achieve a sparse estimate of Ω is the graphical lasso (Friedman et al., 2007; Yuan and Lin, 2007), where the objective function is composed of the negative Gaussian log-likelihood and an ℓ_1 -penalty term for the off-diagonal entries of the inverse covariance matrix over the space of positive definite matrices. This objective function is also proportional to the posterior density of Ω under Laplace priors for the off-diagonal entries, leading to a Bayesian inference and analysis framework (Wang, 2012). Note that the requirement on the positive definiteness of Ω translates to the expensive computational need of inverting $(p-1) \times (p-1)$ matrices in each iteration of both graphical lasso or Bayesian Markov Chain Monte Carlo (MCMC) algorithms.

To mitigate this issue, Khare et al. (2015) relaxed the parameter space of Ω from positive definite matrices to symmetric matrices with positive diagonal entries. Note that it cannot be achieved under the graphical lasso framework due to the determinant of Ω in the likelihood function. Let $S = n^{-1} \sum_{i=1}^n X_i X_i^T$ denote the sample covariance matrix. They introduced the CONvex CORrelation selection methoD (CONCORD) generalized likelihood function, for a given $p \times p$ symmetric matrix Ω ,

$$\begin{aligned} \mathcal{L}(\Omega) &= \exp \left\{ n \sum_{j=1}^p \log \omega_{jj} - \frac{n}{2} \text{tr}(\Omega^2 S) \right\} \\ &= \exp \left\{ n \sum_{j=1}^p \log \omega_{jj} - \frac{1}{2} \sum_{j=1}^p \sum_{i=1}^n \left(\omega_{jj} x_{ij} + \sum_{k \neq j} \omega_{jk} x_{ik} \right)^2 \right\}, \end{aligned} \quad (2.3)$$

which is motivated by the regression-based neighborhood selection method (Meinshausen and Bühlmann, 2006). The quadratic nature of the objective function (2.3) and the

relaxation of the parameter space lead to an entire order of magnitude decrease in computational complexity compared to that required by graphical lasso-based approaches. Hereafter, we proceed with the CONCORD generalized likelihood (2.3) instead of the Gaussian likelihood corresponding to (2.2), and show that asymptotic properties as well as the computational efficiency can be achieved under the Bayesian framework of joint inference.

2.2 Spike and Slab Priors for Graph Selection

The main goal of this paper is to simultaneously infer the sparsity pattern in both β and Ω . To facilitate this purpose, we adopt the prior on precision matrix Ω suggested by Jalali et al. (2020). Specifically, we first introduce the following spike and slab priors for every off-diagonal entry of Ω ,

$$\omega_{jk} \stackrel{ind}{\sim} (1 - q)\delta_0(\omega_{jk}) + qN(0, 1/\lambda_{jk}) \quad \text{for } 1 \leq j < k \leq p, \tag{2.4}$$

where $\delta_0(\cdot)$ denotes the point mass at 0, $\lambda_{jk} > 0$ is the precision of slab part, and $q \in (0, 1)$ is the prior inclusion probability. For the diagonal entries of Ω , we assume

$$\omega_{jj} \stackrel{ind}{\sim} \text{Exp}(\lambda_j) \quad \text{for } 1 \leq j \leq p, \tag{2.5}$$

where $\lambda_j > 0$. Let $\xi = (\omega_{jk}, 1 \leq j < k < p)^T \in \mathbb{R}^{\binom{p}{2}}$ and $\delta = (\omega_{11}, \omega_{22}, \dots, \omega_{pp})^T \in \mathbb{R}^p$ be the collection of all the off-diagonal and diagonal entries of Ω , respectively. Let a symmetric matrix $G = (G_{jk}) \in \{0, 1\}^{p \times p}$ with zero diagonals represent the adjacency matrix corresponding to the precision matrix Ω where $G_{jk} = G_{kj} = 1$ if and only if $\omega_{jk} \neq 0$, and $G_{jk} = G_{kj} = 0$ otherwise. If we further restrict our analysis to only realistic models, i.e., precision matrices with nonzero entries no more than $R_1 > 0$, spike and slab priors (2.4) can be alternatively represented as

$$\begin{aligned} \xi \mid G &\sim N_{|G|}(0, \Lambda_u), \\ \pi(G) &\propto q^{|G|}(1 - q)^{\binom{p}{2} - |G|} I(|G| < R_1), \end{aligned}$$

where $|G| = \sum_{j=1}^{p-1} \sum_{k=j+1}^p G_{jk}$ is the number of nonzero entries in the upper triangular part of G , Λ is a diagonal matrix with diagonal entries $\{\lambda_{jk}, 1 \leq j < k < p\}$, and Λ_u is the sub-matrix of Λ after removing the columns and rows corresponding to the zero indices in the upper triangular part of G (Jalali et al., 2020). In the above, $I(\cdot)$ stands for the indicator function.

The main difference of this approach compared to other existing Bayesian methods is that it does not consider the positive definiteness constraint of Ω , which enables us to use *discrete* spike and slab priors for each off-diagonal entry of Ω . This prior, together with the CONCORD generalized likelihood, enables us to calculate $\pi(G_{jk}, \omega_{jk} \mid \Omega_{-jk}, \gamma, X)$ in a closed form. Thus, we can use the entrywise Gibbs sampler described in Section 3.1. In contrast, for example, Wang (2015) used *continuous* spike and slab priors for each off-diagonal entry of Ω under the positive definiteness constraint. Due to the constraint, it does not allow a closed form of $\pi(G_{jk}, \omega_{jk} \mid \Omega_{-jk}, \gamma, X)$, and the

entrywise Gibbs sampler cannot be used in this case. Wang (2015) instead used the blocked Gibbs sampler that samples each column of Ω in turn. This is indeed more efficient and scalable compared to other traditional Bayesian methods, but requires inversions of $(p-1) \times (p-1)$ matrices to sample each column of Ω , which causes heavy computation for large p .

2.3 Incorporating Graph Structure for Variable Selection

We denote a variable indicator $\gamma = \{\gamma_1, \gamma_2, \dots, \gamma_p\}$ such that $\gamma_j = 1$ if and only if $\beta_j \neq 0$, for $1 \leq j \leq p$. Let $\beta_\gamma \in \mathbb{R}^{|\gamma|}$ be the vector formed by the active components in β corresponding to model γ , where $|\gamma| = \sum_{j=1}^p \gamma_j$ is the number of nonzero entries in γ . For any matrix $A \in \mathbb{R}^{n \times p}$ with p columns, let $A_\gamma \in \mathbb{R}^{n \times |\gamma|}$ represent the submatrix formed from the columns of A corresponding to the nonzero indices in model γ .

For variable selection, we consider the following hierarchical prior over β :

$$\beta_\gamma \mid \gamma \sim N_{|\gamma|}(0, \tau^2 I_{|\gamma|}), \quad (2.6)$$

$$\pi(\gamma \mid G) \propto \exp(-a|\gamma| + b\gamma^T G \gamma) I(|\gamma| < R_2), \quad (2.7)$$

for some constants $a > 0$, $b \geq 0$ and a positive integer $0 \leq R_2 \leq p$. Prior (2.6) can be seen as a collection of slabs of spike and slab priors for regression coefficients (Narisetty and He, 2014; Yang et al., 2016), where τ^2 is the variance of the slab. Prior (2.7) is called an MRF prior on the variable indicator γ . It encourages the inclusion of variables connected to other variables through the adjacency matrix G . MRF priors have been used in the variable selection literature including Peterson et al. (2016); Li and Zhang (2010) and Stingo and Vannucci (2010). Note that the hyperparameter a in (2.7) corresponds to a penalty for large models, and b determines how strongly an adjacency matrix G affects inclusion probabilities of variables. We can jointly infer a variable indicator γ and an adjacency matrix G by considering $b > 0$, whereas $b = 0$ leads to a separate inference of γ and G .

3 Posterior Computation

Model (2.1) is equivalent to letting $Y_i = I(Z_i \geq 0)$, where Z_i is an underlying continuous variable that has a normal distribution with mean $X_i^T \beta$ and variance 1 (Albert and Chib, 1993). As we shall demonstrate subsequently, one can exploit this reparameterization to formulate a Gibbs sampler for posterior inference. Let $Z = (Z_1, Z_2, \dots, Z_n)^T$. Combining this with the CONCORD generalized likelihood (2.3) and priors (2.4)–(2.7), the full posterior of Z, β, γ, Ω and G is given by

$$\begin{aligned} & \pi(Z, \beta, \gamma, \Omega, G \mid Y, X) \\ & \propto \exp\left\{-\frac{1}{2}(Z - X_\gamma \beta_\gamma)^T (Z - X_\gamma \beta_\gamma)\right\} \prod_{i=1}^n \{Y_i I(Z_i \geq 0) + (1 - Y_i) I(Z_i < 0)\} \\ & \times \pi(\gamma \mid G) \prod_{j:\gamma_j=1} (2\pi\tau^2)^{-1/2} \exp\{-\beta_j^2/(2\tau^2)\} \prod_{j:\gamma_j=0} I(\beta_j = 0) \end{aligned}$$

$$\begin{aligned} & \times \exp \left\{ n \sum_{j=1}^p \log \omega_{jj} - \frac{1}{2} \sum_{j=1}^p \sum_{i=1}^n \left(\omega_{jj} x_{ij} + \sum_{k \neq j} \omega_{jk} x_{ik} \right)^2 - \sum_{j=1}^p \lambda_j \omega_{jj} \right\} \\ & \times \pi(G) \prod_{1 \leq j < k \leq p} \left\{ (1 - G_{jk}) \delta_0(\omega_{jk}) + G_{jk} \lambda_{jk}^{1/2} / (2\pi)^{1/2} \exp \left(- \lambda_{jk} \omega_{jk}^2 / 2 \right) \right\}. \end{aligned}$$

For the selection of shrinkage parameters λ_{jk} and λ_j , following Park and Casella (2008) and Jalali et al. (2020), we assign independent gamma prior distributions on each shrinkage parameter, i.e., $\lambda_{jk} \sim \text{Gamma}(r, s)$ for $1 \leq j < k \leq p$ and $\lambda_j \sim \text{Gamma}(r, s)$ for $1 \leq j \leq p$, where r and s are some fixed positive hyperparameters.

3.1 Gibbs Sampler

We suggest using the standard Gibbs sampling for posterior inference. In particular, when sampling the off-diagonal entries of Ω and G , we modify the entrywise Gibbs sampler proposed by Jalali et al. (2020) due to the MRF prior. For any matrix $A = (a_{jk}) \in \mathbb{R}^{p \times p}$ and $1 \leq j \leq k \leq p$, let A_{-jk} denote all the upper triangular entries of A , including diagonals, except a_{jk} . For $1 \leq j \leq p$, let $\beta_{-j} \in \mathbb{R}^{p-1}$ and $X_{-j} \in \mathbb{R}^{n \times (p-1)}$ denote the β vector without the j th predictor and the submatrix of X corresponding to β_{-j} , respectively. Let $\tilde{X}_j \in \mathbb{R}^n$ be the j th column of X . The above full posterior leads to the following Gibbs sampler.

- For $1 \leq i \leq n$, generate Z_i via the following conditional distribution,

$$\pi(Z_i | Y, X, \beta) \propto \begin{cases} N(Z_i | X_i^T \beta, 1) \mathbb{1}(Z_i > 0), & \text{if } Y_i = 1, \\ N(Z_i | X_i^T \beta, 1) \mathbb{1}(Z_i < 0), & \text{if } Y_i = 0. \end{cases}$$

- For $1 \leq j \leq p$, set $\gamma_j = 0$ if $|\gamma_{-j}| = R_2 - 1$. Otherwise, generate γ_j from the conditional distribution,

$$\gamma_j | X, Z, G, \gamma_{-j}, \beta_{-j} \sim \text{Bernoulli} \left(\frac{d_j}{1 + d_j} \right),$$

where $d_j = (\sigma_j / \tau^2)^{1/2} \exp \{ -a + 2b \sum_{i \neq j} \gamma_i G_{ij} + \mu_j^2 / (2\sigma_j) \}$, $\sigma_j = (\tilde{X}_j^T \tilde{X}_j + \tau^{-2})^{-1}$ and $\mu_j = \sigma_j \tilde{X}_j^T (Z - X_{-j} \beta_{-j})$.

- For $1 \leq j \leq p$, generate β_j based on the following spike and slab distribution,

$$\beta_j | X, Z, G, \gamma_j, \beta_{-j} \sim (1 - \gamma_j) \delta_0 + \gamma_j N(\mu_j, \sigma_j).$$

- For $1 \leq j < k \leq p$, set $G_{jk} = 0$ if $|G_{-jk}| = R_1 - 1$. Otherwise, generate G_{jk} based on

$$G_{jk} | \Omega_{-jk}, \gamma, X \sim \text{Bernoulli} \left(\frac{c_{jk}}{1 + c_{jk}} \right),$$

where $S = n^{-1} \sum_{i=1}^n X_i X_i^T = (s_{jk})$ and

$$a_{jk} = s_{jj} + s_{kk} + \frac{\lambda_{jk}}{n}, \quad b_{jk} = \sum_{k' \neq k} \omega_{jk'} s_{kk'} + \sum_{j' \neq j} \omega_{j'k} s_{jj'},$$

$$c_{jk} = \frac{q}{1-q} \left(\frac{\lambda_{jk}}{na_{jk}} \right)^{\frac{1}{2}} \exp \left(\frac{nb_{jk}^2}{2a_{jk}} + 2b\gamma_j \gamma_k \right).$$

- For $1 \leq j < k \leq p$, generate ω_{jk} based on the following spike and slab distribution,

$$\omega_{jk} \mid G_{jk}, \Omega_{-jk}, \gamma, X \sim (1 - G_{jk}) \delta_0(\omega_{jk}) + G_{jk} N \left(-\frac{b_{jk}}{a_{jk}}, \frac{1}{na_{jk}} \right).$$

- For $1 \leq j < k \leq p$, the conditional distribution of λ_{jk} is given by

$$\lambda_{jk} \mid \Omega \sim \text{Gamma}(r + 1/2, \omega_{jk}^2/2 + s).$$

- For $1 \leq j \leq p$, the conditional distribution of λ_j is given by

$$\lambda_j \mid \omega_{jj} \sim \text{Gamma}(r + 1, \omega_{jj} + s). \quad (3.1)$$

- For $1 \leq j \leq p$, the conditional distribution of ω_{jj} is $\pi(\omega_{jj} \mid \Omega_{-jj}, X) \propto \omega_{jj}^n \exp \left\{ -ns_{jj}\omega_{jj}^2/2 - \omega_{jj}(\lambda_j + nb_j) \right\}$, whose normalizing constant is intractable, where $b_j = \sum_{j' \neq j} \omega_{jj'} s_{jj'}$. As suggested by Jalali et al. (2020), we set ω_{jj} as the unique mode of $\pi(\omega_{jj} \mid \Omega_{-jj}, X)$,

$$\omega_{jj}^* = \frac{-(\lambda_j + nb_j) + \sqrt{(\lambda_j + nb_j)^2 + 4n^2 s_{jj}}}{2ns_{jj}}. \quad (3.2)$$

When sampling γ_j and G_{jk} , we are using the conditional posteriors after integrating out β_j and ω_{jk} respectively, rather than using the full conditional posterior. This is to ensure that the Markov chain will be irreducible and converge, where the same trick has been commonly used, for examples, in Yang and Narisetty (2020) and Xu and Ghosh (2015).

Remark 1. An extensive numerical study conducted by Jalali et al. (2020) showed that $\pi(\omega_{jj} \mid \Omega_{-jj}, X)$ puts most of its mass around the mode (3.2). By using this fact, we simply approximate the nonstandard density using the degenerate distribution at the mode for fast inference. Otherwise, one can employ a Metropolis-Hastings algorithm to obtain samples from $\pi(\omega_{jj} \mid \Omega_{-jj}, X)$.

4 Theoretical Properties

For any positive sequences a_n and b_n , we denote (i) $a_n \gg b_n$ if $a_n/b_n \rightarrow \infty$ as $n \rightarrow \infty$, (ii) $a_n = O(b_n)$ if there exists a constant $C > 0$ such that $a_n/b_n \leq C$ for all large n , (iii) $a_n \sim b_n$ if $a_n = O(b_n)$ and $b_n = O(a_n)$ as $n \rightarrow \infty$, and (iv) $a_n = o(b_n)$ if

$a_n/b_n \rightarrow 0$ as $n \rightarrow \infty$, For any $a = (a_1, a_2, \dots, a_p)^T \in \mathbb{R}^p$, we denote vector norms by $\|a\|_1 = \sum_{j=1}^p |a_j|$, $\|a\|_2 = (\sum_{j=1}^p a_j^2)^{1/2}$ and $\|a\|_{\max} = \max_{1 \leq j \leq p} |a_j|$. For any $p \times p$ matrix A , let $\lambda_{\min}(A)$ and $\lambda_{\max}(A)$ be the minimum and maximum eigenvalues of A , respectively.

In this section, we investigate asymptotic theoretical properties of the proposed Bayesian joint variable and graph selection method. We are interested in whether the joint posterior for the variable and graph is concentrated on each true value. Let $\beta_0 = (\beta_{0,j}) \in \mathbb{R}^p$ be the true coefficient vector, and $\gamma_0 = (\gamma_{0,j}) \in \{0, 1\}^p$ be the binary vector indicating locations of nonzero entries in β_0 , i.e., $\gamma_{0,j} = I(\beta_{0,j} \neq 0)$ for $j = 1, 2, \dots, p$. Let $\Omega_0 = (\omega_{0,jk}) \in \mathbb{R}^{p \times p}$ be the true precision matrix of X_i , and $G_0 = (G_{0,jk}) \in \{0, 1\}^{p \times p}$ be the corresponding adjacency matrix. Based on these quantities, we assume that the true data-generating mechanism is $Y_i | X_i, \beta_0 \stackrel{ind}{\sim} \text{Ber}(\Phi(X_i^T \beta_0))$ with a random predictor vector X_i such that $\text{Cov}(X_i) = \Omega_0^{-1}$, for $i = 1, 2, \dots, n$. The following assumptions were made in order to demonstrate the theoretical properties. In the below, \mathbb{P}_0 and \mathbb{E}_0 denote the probability measure and expectation, respectively, under the true data-generating mechanism.

Condition (A1) (Conditions on n and p) $p = p_n \geq n$ and $\log p = o(n)$ as $n \rightarrow \infty$.

Condition (A2) (Conditions on the design matrix) For $X_i \in \mathbb{R}^p$, $i = 1, 2, \dots, p$, we assume the following:

- (i) (sub-gaussianity) There exists a constant $C > 0$ such that $\mathbb{E}_0 \exp(\alpha^T X_i) \leq \exp(C\|\alpha\|_2^2)$ for all $\alpha \in \mathbb{R}^p$.
- (ii) (bounded eigenvalues) There exists a constant $0 < \epsilon_0 < 1$ such that $\epsilon_0 \leq \lambda_{\min}(\Omega_0) \leq \lambda_{\max}(\Omega_0) \leq \epsilon_0^{-1}$.
- (iii) (boundedness) $\mathbb{P}_0(\|X_i\|_{\max} \leq M) = 1$ for some constant $M > 0$.

Condition (A3) (Conditions on β_0) $|\gamma_0| = O(1)$, $\|\beta_0\|_1 = O(1)$ and $\beta_{0,\min}^2 \equiv \min_{j \in \gamma_0} \beta_{0,j}^2 \geq C_{\beta_0} \log p/n$ for some constant $C_{\beta_0} > 0$.

Condition (A4) (Conditions on Ω_0) $(|G_0| + 1)^2 \log p = o(n)$ and $\Omega_{0,\min} \equiv \min_{(j,k): G_{0,jk}=1} \omega_{0,jk}^2 \gg \{|G_0| \log p + (\log n)/2\}/n$.

Condition (A5) (Conditions on the hyperparameter q) $q = p^{-C_q |G_0|}$, where $C_q = 16(1 \vee c_0)^2 / (1 \wedge \epsilon_0)$, for some constant $c_0 > 0$ defined in Lemma S3 of Jalali et al. (2020).

Condition (A6) (Conditions on the other hyperparameters) For some constants $1/2 < d < 1$, $\delta > 0$ and $C_a > 0$, $R_1 = (n/\log p)^{1/2}$, $R_2 = (n/\log p)^{1/2-d}$, $\tau^2 \sim n^{-1} p^{2+2\delta}$, $a = C_a \log p$ and $b = o((\log p/n)^{1-d})$.

Condition (A1) demonstrates the high-dimensional setting, where the number of variables p is larger than the sample size n . It allows p to grow at a rate $\exp\{o(n)\}$ as $n \rightarrow \infty$. Similar conditions have been used in the literature including Narisetty and He (2014) and Lee and Cao (2021a) to prove selection consistency of coefficient vector.

Condition (A2) shows the conditions for each row, X_i , of the random design matrix X . The first condition implies that a linear combination of $X_i = (x_{i1}, x_{i2}, \dots, x_{ip})^T$ has a sufficiently light tail satisfying sub-gaussianity. The second condition requires that the eigenvalues of precision matrix Ω_0 are bounded. Liu and Martin (2019) and Cao and Lee (2021) also used this condition for linear regression models with random design matrix. The third condition requires each component of X_i is bounded with probability 1, where Narisetty et al. (2019) adopted a similar condition for a deterministic design matrix. By assuming these conditions for X , we can efficiently control the eigenvalues of $n^{-1}X_\gamma^T X_\gamma$ and the Hessian matrix of (2.1) for any reasonably large model γ , with large probability tending to 1. For example, condition (A2) holds if $X_i = \Omega_0^{-1/2} Z_i$, where $Z_i \stackrel{i.i.d.}{\sim} \text{Unif}([- \sqrt{3}, \sqrt{3}]^p)$ for $i = 1, 2, \dots, n$ and $\|\Omega_0\|_1 = O(1)$. Here, $\|\cdot\|_1$ denotes the matrix ℓ_1 -norm.

Condition (A3) means that the true regression coefficient β_0 has finite numbers of nonzero entries and a bounded ℓ_1 -norm. It holds that if we assume $\|\beta_0\|_{\max} = O(1)$. For examples, Johnson and Rossell (2012) and Narisetty and He (2014) assumed similar conditions. Note that we still allow, as the number of variables increases, the magnitude of the smallest coefficient converge to zero at the rate of $\log p/n$. This can describe a situation in which the importance of meaningful variables decreases as the number of variables grows.

Condition (A4) requires the number of nonzero off-diagonal entries in Ω_0 is at most $O(\sqrt{n/\log p})$. Banerjee and Ghosal (2015), Xiang et al. (2015) and Lee and Cao (2021b) used similar conditions for high-dimensional precision matrices. Furthermore, condition (A4) allows the magnitude of the smallest nonzero off-diagonal elements of Ω_0 converge to zero at the rate $(|G_0| \log p + \log n)/n$. We adopt these conditions from Jalali et al. (2020) to use their results.

Among conditions (A5) and (A6), $q = p^{-C_a |G_0|}$ and $a = C_a \log p$ mean that the prior should impose a sufficient penalty to large $|G|$ and $|\gamma|$, respectively. These are standard assumptions for Bayesian inference of high-dimensional precision matrix and regression vector. For examples, see Liu and Martin (2019), Jalali et al. (2020), Cao et al. (2019) and Martin et al. (2017). The condition $\tau^2 \sim n^{-1} p^{2+2\delta}$ implies that the variance of slab part should be sufficiently large, where τ^2 essentially plays a role as a penalty for large $|\gamma|$. The other conditions, $R_1 = (n/\log p)^{\frac{1}{2}}$ and $R_2 = (n/\log p)^{\frac{1-d}{2}}$ control the size of $|G|$ and $|\gamma|$, respectively, while $b = o((\log p/n)^{1-d})$ controls the strength of $\gamma^T G \gamma$ term in $\pi(\gamma | G)$. Similar conditions can be found in Jalali et al. (2020) and Cao and Lee (2021).

With these conditions at hand, we are now ready to state asymptotic properties of the posterior. Theorem 4.1 shows the proposed prior enjoys posterior ratio consistency of γ given any G . This implies that for any fixed G , the true variable indicator γ_0 is the mode of the conditional posterior $\pi(\gamma | G, Y, X)$ with probability tending to 1. Note that consistency of γ is achieved for any G , even with a G very distant from the true G_0 . *Theorem 4.1* (Posterior ratio consistency of γ). Suppose conditions (A1)–(A3) and (A6) hold. Then, for any $\gamma \neq \gamma_0$ and G ,

$$\frac{\pi(\gamma, G | Y, X)}{\pi(\gamma_0, G | Y, X)} \xrightarrow{P} 0 \quad \text{as } n \rightarrow \infty.$$

To establish posterior ratio consistency of G given γ_0 , we assume the existence of accurate estimates of diagonal entries $\delta = (\omega_{11}, \omega_{22}, \dots, \omega_{pp})$, say $\hat{\delta} = (\hat{\omega}_{11}, \hat{\omega}_{22}, \dots, \hat{\omega}_{pp})$, satisfying

$$\|\delta - \hat{\delta}\|_{\max} = O(\sqrt{\log p/n}) \tag{4.1}$$

with probability at least $1 - n^{-c}$ for any constant $c > 0$. The existence of these estimates have been commonly assumed for high-dimensional precision matrix estimation (Peng et al., 2009; Khare et al., 2015); for example, Proposition 1 in Peng et al. (2009) provides one way to obtain such estimates of δ . Because our main focus is selection of γ and G , not the estimation of Ω , we will work with the conditional posterior of γ and G with the estimates $\hat{\delta}$ plugged in. The next theorem states the posterior ratio consistency result of G given γ_0 and $\hat{\delta}$, which implies the true graph G_0 is the mode of $\pi(G \mid \gamma_0, \hat{\delta}, Y, X)$ with probability tending to 1.

Theorem 4.2 (Posterior ratio consistency of G). Suppose conditions (A2), (A4), (A5) and $|\gamma_0| = O(1)$ hold. Assume that the existence of accurate estimates of diagonal entries satisfying (4.1). Then, for any $G \neq G_0$,

$$\frac{\pi(\gamma_0, G \mid \hat{\delta}, Y, X)}{\pi(\gamma_0, G_0 \mid \hat{\delta}, Y, X)} \xrightarrow{P} 0 \quad \text{as } n \rightarrow \infty.$$

For any γ and G , note that

$$\begin{aligned} \frac{\pi(\gamma, G \mid Y, X)}{\pi(\gamma_0, G \mid Y, X)} &= \frac{f(Y \mid X_\gamma, \gamma)\pi(X \mid G)\pi(\gamma \mid G)\pi(G)}{f(Y \mid X_{\gamma_0}, \gamma_0)\pi(X \mid G)\pi(\gamma_0 \mid G)\pi(G)} \\ &= \frac{f(Y \mid X_\gamma, \gamma)\pi(X \mid \hat{\delta}, G)\pi(\gamma \mid G)\pi(G)}{f(Y \mid X_{\gamma_0}, \gamma_0)\pi(X \mid \hat{\delta}, G)\pi(\gamma_0 \mid G)\pi(G)} = \frac{\pi(\gamma, G \mid \hat{\delta}, Y, X)}{\pi(\gamma_0, G \mid \hat{\delta}, Y, X)}, \end{aligned}$$

where $f(Y \mid X_\gamma, \gamma) = \int f(Y \mid X_\gamma, \beta_\gamma)\pi(\beta_\gamma \mid \gamma)d\beta_\gamma$, $\pi(X \mid G) = \int \pi(X \mid \Omega, G)\pi(\Omega \mid G)d\Omega$ and $\pi(X \mid \hat{\delta}, G) = \int \pi(X \mid \xi, \hat{\delta}, G)\pi(\xi \mid G)d\xi$. Then, by using the above equality, Theorems 4.1 and 4.2 imply joint posterior ratio consistency of γ and G . Corollary 4.3 states the joint selection consistency result.

Corollary 4.3 (Joint posterior ratio consistency of γ and G). Suppose conditions (A1)–(A6) hold. Assume that the existence of accurate estimates of diagonal entries satisfying (4.1). Then, $\gamma \neq \gamma_0$ and $G \neq G_0$,

$$\frac{\pi(\gamma, G \mid \hat{\delta}, Y, X)}{\pi(\gamma_0, G_0 \mid \hat{\delta}, Y, X)} \xrightarrow{P} 0 \quad \text{as } n \rightarrow \infty.$$

In fact, the proposed method enjoys called joint selection consistency. Theorem 4.4 shows that the joint posterior of γ and G given $\hat{\delta}$ is concentrated around the true values, γ_0 and G_0 . Joint selection consistency guarantees that the posterior mass assigned to γ_0 and G_0 converges to 1 as $n \rightarrow \infty$. This is a more powerful result than Corollary 4.3, because joint selection consistency implies joint posterior ratio consistency, but not vice versa.

Theorem 4.4 (Joint selection consistency of γ and G). Suppose conditions (A1)–(A6) hold. Assume that the existence of accurate estimates of diagonal entries satisfying (4.1).

Then,

$$\pi(\gamma_0, G_0 \mid \hat{\delta}, Y, X) \xrightarrow{P} 1 \quad \text{as } n \rightarrow \infty.$$

5 Simulation Studies

In this section, we demonstrate the performance of the proposed method in various settings. For $i = 1, 2, \dots, n$, we simulate the data from $Y_i = I(Z_i \geq 0)$, where $Z_i = X_i\beta_0 + \epsilon_i$, $\epsilon_i \sim N(0, 1)$ and $X_i = (x_{i1}, x_{i2}, \dots, x_{ip})^T \stackrel{i.i.d.}{\sim} N_p(0, \Sigma_0)$, with the sample size n and the number of predictors p . Throughout the simulation study, we fix $n = 100$. If the atlas segments the brain into p different anatomical sections, then, for example, we can consider p as the number of brain regions. In this case, the objective of joint inference would be to learn the abnormal functional activities among the significant brain regions that contribute to the disease onset.

Among these p predictors, we assume that the first ten are active and consider the following six settings for the true coefficient vector β_0 to include different combinations of small and large signals.

- Setting 1: Generate β_{0,γ_0} from $\text{Unif}(-3, -1.5)$.
- Setting 2: Generate β_{0,γ_0} from $\text{Unif}(1.5, 3)$.
- Setting 3: Generate β_{0,γ_0} from $\text{Unif}((-3, -1.5) \cup (1.5, 3))$.
- Setting 4: Generate β_{0,γ_0} from $\text{Unif}(0.5, 1.5)$.
- Setting 5: Generate β_{0,γ_0} from $\text{Unif}(-1.5, -0.5)$.
- Setting 6: Generate β_{0,γ_0} from $\text{Unif}((-1.5, -0.5) \cup (0.5, 1.5))$.

For the true precision matrix $\Omega_0 = \Sigma_0^{-1}$, we consider the following four scenarios.

- Scenario 1: For $p = 150$, we set all the diagonal entries to be 1 and $\Omega_{0,i1} = \Omega_{0,1i} = 0.3$ for $i = 2, 3, \dots, 10$, and set all the remaining entries to be 0.
- Scenario 2: For $p = 150$, we consider a banded structure of Ω_0 with all the unit diagonals, where $\Omega_{0,i,i+1} = \Omega_{0,i+1,i} = 0.3$, for $i = 1, 2, \dots, p - 1$.
- Scenario 3: For $p = 150$, we consider another banded structures of Ω_0 with all the unit diagonals, where $\Omega_{0,i,i+1} = \Omega_{0,i+1,i} = 0.5$, $\Omega_{0,j,j+2} = \Omega_{0,j+2,j} = 0.25$, for $i = 1, 2, \dots, p - 1, j = 1, 2, \dots, p - 2$.
- Scenario 4: The true precision matrix Ω_0 is set to be the same as in Scenario 1, but with $p = 300$. This scenario will show the performance of the proposed method in high dimensions.

Lastly, we consider a scenario where both the inverse covariance matrix and the true regression coefficient possess a lower degree of sparsity compared with previous

settings. Specifically, we generate the covariates $X_i \stackrel{i.i.d.}{\sim} N_p(0, \Sigma_0), i = 1, \dots, n$, where $n = 100, p = 150, \Sigma_0 = \tilde{\Sigma}_0 + \{0.01 - \lambda_{\min}(\tilde{\Sigma}_0)\}I_p$ and

$$(\tilde{\Sigma}_0)_{ij} = \begin{cases} 2 \max(1 - \frac{|i-j|}{10}, 0), & \text{if } |i - j| \leq 5, \\ 0, & \text{otherwise,} \end{cases}$$

which results in roughly 25% of the entries in Ω_0 being nonzero. Next, for the true regression coefficient vector, we consider the first 20 entries of β_0 to be active and their magnitudes are set as in Settings 1 to 4. We call this simulation setup Scenario 5, and the results for this setting are reported at Table 5.

We will refer to our proposed joint selection method coupled with Bayesian spike and slab CONCORD as J.BSSC (Joint Bayesian Spike and Slab Concord). In terms of variable selection, we first compare the performance of J.BSSC with other existing methods including Lasso (Tibshirani, 1996), elastic net (Zou and Hastie, 2005) and the Bayesian joint selection method based on stochastic search structure learning (SSSL) (Peterson et al., 2016; Wang, 2015), hereafter referred to as J.SSSL.

The tuning parameters in Lasso and elastic net were chosen by 10-fold cross-validation. For Bayesian methods, as discussed by Peterson et al. (2016), we suggest using the hyperparameters $a = 2.75$ and $b = 0.5$ for the MRF prior as default, but we also tune the value of a over a grid from 2 to 2.75 and the value of b from 0.1 to 0.5 based on cross-validation. Furthermore, to show the benefits of joint modeling, we also implement the setting with $b = 0$ for J.BSSC, which corresponds to the Bayesian method modeling the variable and precision matrix separately. The other hyperparameters were set at $a_0 = 0.1, b_0 = 0.01, \tau^2 = 1, q = 0.005, r = 10^{-4}$ and $s = 10^{-8}$. The initial state for γ was set at p -dimensional zero vector, i.e., the empty model, while the initial state for the inverse covariance matrix was chosen by the graphical lasso (GLasso) (Friedman et al., 2007). For posterior inference, 2,000 posterior samples were drawn with a burn-in period of 2,000. As the final model, we chose the indices having posterior inclusion probability larger than 0.5, which is called the median probability model. When the posterior probability of the posterior mode is larger than 0.5, the median probability model corresponds to the posterior mode (Barbieri and Berger, 2004). The R code implementing the proposed J.BSSC is publicly available at <https://github.com/xuancao/Joint-Selection-in-Probit-Regression>.

To evaluate the performance of variable selection, the sensitivity, specificity, Matthews correlation coefficient (MCC) and mean-squared prediction error (MSPE) are reported at Tables 1 to 4. The criteria are defined as

$$\begin{aligned} \text{Sensitivity} &= \frac{TP}{TP + FN}, \\ \text{Specificity} &= \frac{TN}{TN + FP}, \\ \text{MCC} &= \frac{TP \times TN - FP \times FN}{\sqrt{(TP + FP)(TP + FN)(TN + FP)(TN + FN)}}, \\ \text{MSPE} &= \frac{1}{n_{\text{test}}} \sum_{i=1}^{n_{\text{test}}} \{\Phi(X_{\text{test},i}^T \hat{\beta}) - Y_{\text{test},i}\}^2, \end{aligned}$$

	Setting 1				Setting 2			
	Sensitivity	Specificity	MCC	MSPE	Sensitivity	Specificity	MCC	MSPE
J.BSSC ($b > 0$)	0.72	1	0.83	0.15	0.79	0.99	0.80	0.10
J.BSSC ($b = 0$)	0.42	0.99	0.58	0.23	0.46	1	0.63	0.18
J.SSSL	0.68	0.79	0.27	0.16	0.64	0.76	0.23	0.22
Lasso	0.79	0.97	0.72	0.08	0.80	0.98	0.75	0.12
Elastic	0.98	0.92	0.70	0.20	1	0.94	0.70	0.20
	Setting 3				Setting 4			
	Sensitivity	Specificity	MCC	MSPE	Sensitivity	Specificity	MCC	MSPE
J.BSSC ($b > 0$)	0.78	1	0.84	0.11	0.54	1	0.68	0.17
J.BSSC ($b = 0$)	0.60	1	0.76	0.15	0.31	1	0.54	0.21
J.SSSL	0.74	0.77	0.29	0.23	0.72	0.77	0.27	0.21
Lasso	0.55	0.95	0.46	0.12	0.82	0.98	0.79	0.09
Elastic	0.62	0.79	0.26	0.20	0.84	0.97	0.75	0.19
	Setting 5				Setting 6			
	Sensitivity	Specificity	MCC	MSPE	Sensitivity	Specificity	MCC	MSPE
J.BSSC ($b > 0$)	0.60	1	0.72	0.12	0.64	0.99	0.72	0.13
J.BSSC ($b = 0$)	0.40	1	0.61	0.17	0.21	0.99	0.31	0.23
J.SSSL	0.70	0.79	0.28	0.18	0.64	0.78	0.24	0.17
Lasso	0.76	0.97	0.70	0.10	0.71	0.92	0.48	0.16
Elastic	0.98	0.89	0.61	0.19	0.52	0.93	0.47	0.24

Table 1: The summary statistics for Scenario 1 are represented for different settings, which corresponds to different choice of the true coefficient β_0 .

	Setting 1				Setting 2			
	Sensitivity	Specificity	MCC	MSPE	Sensitivity	Specificity	MCC	MSPE
J.BSSC ($b > 0$)	0.96	1	0.97	0.08	1	1	1	0.05
J.BSSC ($b = 0$)	0.72	1	0.84	0.15	0.88	1	0.90	0.14
J.SSSL	0.87	0.79	0.37	0.22	0.84	0.77	0.34	0.24
Lasso	0.77	0.91	0.49	0.19	0.66	0.90	0.41	0.18
Elastic	0.59	0.84	0.34	0.24	0.50	0.93	0.38	0.24
	Setting 3				Setting 4			
	Sensitivity	Specificity	MCC	MSPE	Sensitivity	Specificity	MCC	MSPE
J.BSSC ($b > 0$)	0.88	1	0.92	0.14	0.90	0.99	0.89	0.11
J.BSSC ($b = 0$)	0.49	0.98	0.53	0.20	0.76	0.99	0.84	0.18
J.SSSL	0.57	0.74	0.17	0.26	0.53	0.77	0.18	0.24
Lasso	0.65	0.91	0.42	0.14	0.61	0.89	0.36	0.17
Elastic	0.78	0.72	0.34	0.23	0.60	0.86	0.32	0.23
	Setting 5				Setting 6			
	Sensitivity	Specificity	MCC	MSPE	Sensitivity	Specificity	MCC	MSPE
J.BSSC ($b > 0$)	0.90	1	0.93	0.11	0.62	0.99	0.70	0.16
J.BSSC ($b = 0$)	0.62	1	0.77	0.19	0.58	1	0.73	0.18
J.SSSL	0.50	0.74	0.13	0.24	0.66	0.79	0.27	0.27
Lasso	0.71	0.89	0.42	0.20	0.72	0.95	0.56	0.15
Elastic	0.83	0.57	0.22	0.24	0.81	0.73	0.32	0.22

Table 2: The summary statistics for Scenario 2 are represented for different settings, which corresponds to different choice of the true coefficient β_0 .

where TP, TN, FP and FN are the true positive, true negative, false positive and false negative, respectively, and $\hat{\beta}$ denotes the estimated coefficient based on each method. For Bayesian methods, the usual GLM estimates based on the selected variables were used as $\hat{\beta}$. We generated test samples and corresponding predictors $Y_{\text{test},1}, Y_{\text{test},2}, \dots, Y_{\text{test},n_{\text{test}}}$ and $X_{\text{test},1}, X_{\text{test},2}, \dots, X_{\text{test},n_{\text{test}}}$, respectively, with $n_{\text{test}} = 50$ to calculate the MSPE.

	Setting 1				Setting 2			
	Sensitivity	Specificity	MCC	MSPE	Sensitivity	Specificity	MCC	MSPE
J.BSSC ($b > 0$)	1	1	0.99	0.05	0.92	1	0.95	0.07
J.BSSC ($b = 0$)	0.42	0.99	0.52	0.22	0.82	0.99	0.85	0.10
J.SSSL	0.50	0.72	0.12	0.25	0.67	0.74	0.23	0.24
Lasso	0.57	0.92	0.38	0.20	0.41	0.94	0.33	0.22
Elastic	0.54	0.83	0.25	0.24	0.48	0.89	0.32	0.24

	Setting 3				Setting 4			
	Sensitivity	Specificity	MCC	MSPE	Sensitivity	Specificity	MCC	MSPE
J.BSSC ($b > 0$)	0.76	1	0.83	0.11	0.80	1	0.85	0.12
J.BSSC ($b = 0$)	0.70	1	0.82	0.13	0.67	0.99	0.73	0.19
J.SSSL	0.52	0.71	0.13	0.25	0.50	0.71	0.12	0.23
Lasso	0.66	0.92	0.45	0.15	0.56	0.92	0.38	0.19
Elastic	0.66	0.85	0.38	0.24	0.55	0.91	0.37	0.23

	Setting 5				Setting 6			
	Sensitivity	Specificity	MCC	MSPE	Sensitivity	Specificity	MCC	MSPE
J.BSSC ($b > 0$)	0.80	0.99	0.82	0.11	0.66	0.99	0.75	0.14
J.BSSC ($b = 0$)	0.51	1	0.70	0.17	0.51	0.98	0.55	0.20
J.SSSL	0.53	0.73	0.15	0.31	0.66	0.73	0.21	0.23
Lasso	0.45	0.90	0.26	0.23	0.53	0.95	0.45	0.12
Elastic	0.38	0.86	0.18	0.24	0.82	0.53	0.19	0.20

Table 3: The summary statistics for Scenario 3 are represented for different settings, which corresponds to different choice of the true coefficient β_0 .

	Setting 1				Setting 2			
	Sensitivity	Specificity	MCC	MSPE	Sensitivity	Specificity	MCC	MSPE
J.BSSC ($b > 0$)	0.58	0.99	0.66	0.18	0.74	1	0.85	0.08
J.BSSC ($b = 0$)	0.40	0.99	0.46	0.18	0.48	1	0.65	0.13
J.SSSL	0.47	0.86	0.18	0.18	0.50	0.87	0.21	0.16
Lasso	0.78	0.97	0.57	0.11	0.73	0.98	0.61	0.06
Elastic	0.94	0.90	0.51	0.21	0.75	0.99	0.77	0.18

	Setting 3				Setting 4			
	Sensitivity	Specificity	MCC	MSPE	Sensitivity	Specificity	MCC	MSPE
J.BSSC ($b > 0$)	0.40	1	0.56	0.13	0.64	1	0.72	0.13
J.BSSC ($b = 0$)	0.22	1	0.45	0.15	0.38	1	0.51	0.16
J.SSSL	0.66	0.86	0.29	0.22	0.43	0.86	0.17	0.13
Lasso	0.74	0.95	0.47	0.15	0.70	0.97	0.60	0.13
Elastic	0.42	0.93	0.37	0.24	0.59	0.99	0.65	0.19

	Setting 5				Setting 6			
	Sensitivity	Specificity	MCC	MSPE	Sensitivity	Specificity	MCC	MSPE
J.BSSC ($b > 0$)	0.56	0.99	0.68	0.15	0.50	1	0.62	0.13
J.BSSC ($b = 0$)	0.30	0.99	0.34	0.21	0.30	0.99	0.41	0.20
J.SSSL	0.62	0.85	0.28	0.18	0.70	0.87	0.32	0.16
Lasso	0.78	0.97	0.58	0.10	0.63	0.92	0.34	0.19
Elastic	0.96	0.78	0.32	0.19	0.70	0.78	0.24	0.23

Table 4: The summary statistics for Scenario 4 are represented for different settings, which corresponds to different choice of the true coefficient β_0 .

The sensitivity, specificity, MCC and MSPE, under different scenarios, are reported at Tables 1–5 to evaluate the variable selection performance. We notice that compared to regularization methods (Lasso and elastic net), the proposed joint selection approach (J.BSSC) tends to have better specificity and MCC. The poor specificity of the regular-

	Setting 1				Setting 2			
	Sensitivity	Specificity	MCC	MSPE	Sensitivity	Specificity	MCC	MSPE
J.BSSC ($b > 0$)	0.56	0.98	0.63	0.15	0.60	0.98	0.68	0.10
J.BSSC ($b = 0$)	0.25	1	0.47	0.25	0.35	0.98	0.48	0.11
J.SSSL	0.44	0.75	0.13	0.28	0.38	0.69	0.06	0.29
Lasso	0.81	0.91	0.62	0.09	0.70	0.93	0.60	0.11
Elastic	1	0.77	0.55	0.19	0.99	0.74	0.53	0.18
	Setting 3				Setting 4			
	Sensitivity	Specificity	MCC	MSPE	Sensitivity	Specificity	MCC	MSPE
J.BSSC ($b > 0$)	0.34	0.99	0.50	0.22	0.55	0.98	0.62	0.12
J.BSSC ($b = 0$)	0.22	0.97	0.29	0.27	0.30	0.98	0.43	0.20
J.SSSL	0.33	0.67	0.01	0.28	0.48	0.73	0.16	0.24
Lasso	0.62	0.80	0.33	0.14	0.71	0.91	0.56	0.12
Elastic	0.82	0.57	0.28	0.21	1	0.71	0.50	0.18
	Setting 5				Setting 6			
	Sensitivity	Specificity	MCC	MSPE	Sensitivity	Specificity	MCC	MSPE
J.BSSC ($b > 0$)	0.41	1	0.57	0.19	0.27	0.98	0.41	0.21
J.BSSC ($b = 0$)	0.25	1	0.47	0.26	0.21	0.99	0.37	0.24
J.SSSL	0.46	0.73	0.14	0.26	0.42	0.69	0.08	0.25
Lasso	0.58	0.89	0.41	0.13	0.48	0.82	0.25	0.18
Elastic	0.80	0.66	0.32	0.19	0.73	0.77	0.38	0.22

Table 5: The summary statistics for Scenario 5 are represented for different settings, which corresponds to different choice of the true coefficient β_0 .

ization methods has also been discussed in previous literature in the sense that selection of the regularization parameter using cross-validation is optimal with respect to prediction but tends to include too many noise predictors (Meinshausen and Bühlmann, 2006). This leads to relatively larger numbers of errors for the regularization methods compared with those for the Bayesian joint selection methods. This pattern becomes more noticeable in Scenario 5 as a large number of beta entries are set to nonzero. Note that in our theoretical analysis, we assume the true complexity of γ_0 to be finite compared with the increasing dimension, suggesting our proposed method may prefer a relatively sparse setting. Among all Bayesian approaches, under most of settings, the proposed J.BSSC approach (with $b > 0$ or $b = 0$) outperforms J.SSSL based on all criteria, which shows the benefit of the proposed joint method incorporating the graph structure through the CONCORD generalized likelihood. Interestingly, compared with J.SSSL that adopts the Metropolis-Hastings algorithm for variable selection, the performance of the proposed Gibbs sampler is significantly better in terms of almost all the measures. Furthermore, J.BSSC with $b > 0$ tends to have a slightly lower specificity but significantly higher sensitivity, MCC and lower MSPE compared with J.BSSC with $b = 0$. This could be caused by the proposed method frequently visiting graph-linked variables due to the MRF prior. We also found that the proposed J.BSSC overall works better in the strong signal settings where the signs of all true nonzero coefficients are consistent (i.e., Settings 1 and 2) compared with other settings. This is because as signal strength gets stronger, the consistency conditions of our method are easier to satisfy which leads to better performance. To sum up, the above observation indicates that the proposed method can achieve good variable selection performance under a variety of configurations with different data generation mechanisms.

Variable	Classification		Inclusion probability		True classification
	J.BSSC	J.SSSL	J.BSSC	J.SSSL	
γ_2	Nonzero	Zero	1	0.01	Nonzero
γ_3	Nonzero	Zero	0.96	0	Nonzero
γ_{11}	Zero	Nonzero	0.03	0.69	Zero
$G_{35,9}$	Zero	Nonzero	0.01	0.78	Zero
$G_{130,52}$	Zero	Nonzero	0.10	0.57	Zero
$G_{136,115}$	Zero	Nonzero	0.21	0.98	Zero
$(\gamma_2, G_{2,1})$	Nonzero	Zero	1	0.01	Nonzero
$(\gamma_3, G_{3,1})$	Nonzero	Zero	0.96	0	Nonzero
$(\gamma_6, G_{6,1})$	Nonzero	Nonzero	1	0.76	Nonzero

Table 6: Illustration of classification based on marginal and joint posterior inclusion probabilities using J.BSSC and J.SSSL for selected entries of γ and G .

n	p	Sensitivity	Specificity	MCC
50	75	1	1	1
50	100	1	1	1
100	150	1	1	1
100	200	1	1	1
150	225	1	1	1
150	300	0.96	1	0.98

Table 7: The summary statistics for variable selection with varying dimensions averaged over 20 replicates for J.BSSC.

Next, we illustrate the uncertainty quantification for J.BSSC and J.SSSL using marginal as well as joint inclusion probabilities. We first consider the simulation setup under Setting 1, Scenario 1, and randomly choose one out of the 20 replicated data sets. Table 6 shows the estimated inclusion probabilities for selected entries in γ and G using both the J.BSSC method and the J.SSSL approach. Entries γ_{11} , $G_{35,9}$, $G_{130,52}$, and $G_{136,115}$ are all falsely identified as nonzero by J.SSSL based on inclusion probabilities greater than 0.5, but correctly identified as zero by J.BSSC. Entries γ_2 , γ_3 along with pairs of $(\gamma_2, G_{2,1})$ and $(\gamma_3, G_{3,1})$ are correctly identified as nonzero by J.BSSC while J.SSSL incorrectly identifies those as zero with inclusion probabilities close or equal to 0. The last entry corresponding to the pair of $(\gamma_6, G_{6,1})$ is correctly identified as nonzero by both methods, but J.SSSL has a lower inclusion probability. The pattern reflected in Table 6 is consistent with the significantly better selection performance of J.BSSC compared with J.SSSL.

We also conduct another simulation study under Setting 2 and the covariance structure specified in Scenario 2 to examine the selection performance of J.BSSC with increasing dimensions as stated in our technical assumption. The sparsity level is set at $p/30$ and the results are given in Table 7. We can tell that as dimension grows, our method is able to consistently recover the true signals under sparse settings.

We also briefly present the performance of graph selection and precision matrix estimation for J.BSSC. We compare the performance of J.BSSC with other existing methods

	Sensitivity	Specificity	MCC	#Error
J.BSSC	1	1	0.90	2
J.SSSL	1	1	0.87	3
GLasso	1	0.98	0.19	239
CLIME	1	0.98	0.18	256
TIGER	1	1	0.73	8

Table 8: The summary statistics for graph selection under Setting 1 and Scenario 1 are represented.

	E_1	E_2	E_3	E_4
J.BSSC	0.13	0.21	0.08	0.28
J.SSSL	8.01	7.26	1.86	11.95
GLasso	0.37	0.24	0.19	0.19
CLIME	1.51	2.22	0.58	4.16
TIGER	1.47	1.91	0.31	3.48

Table 9: The summary statistics for precision matrix estimation under Setting 1 and Scenario 1 are represented.

including J.SSSL (Peterson et al., 2016; Wang, 2015), GLasso (Friedman et al., 2007), the constrained ℓ_1 -minimization for inverse matrix estimation (CLIME) (Cai et al., 2011) and the tuning-insensitive approach for optimally estimating Gaussian graphical models (TIGER) (Liu and Wang, 2017). The tuning parameters for GLasso and TIGER were chosen by the criterion of stability approach to regularization selection (StARS) (Liu et al., 2010). We used 10-fold cross-validation to select the penalty parameter for CLIME. For GLasso and TIGER, the final models were constructed by collecting the nonzero entries in the estimated precision matrix. In our simulation settings, CLIME could not produce exact zeros, so we chose the final graph estimate by thresholding the absolute values of the estimated precision matrix at 0.1.

To evaluate the performance of graph selection and precision matrix estimation, we report the results at Tables 8 and 9, where each simulation setting is repeated for 20 times. The results under different scenarios are omitted because they gave similar conclusions, and only the results under Scenario 1 are presented in the tables. In Table 8, #Error denotes the number of errors, i.e., FP+FN. For a matrix norm $\|\cdot\|$ and an estimator $\hat{\Omega}$, the relative error $\|\Omega_0 - \hat{\Omega}\|/\|\Omega_0\|$ is chosen as a criterion. In Table 9, E_1 , E_2 , E_3 and E_4 represent the relative errors based on the matrix ℓ_1 -norm, the matrix ℓ_2 -norm (spectral norm), the vector ℓ_2 -norm (Frobenius norm) and the vector ℓ_∞ -norm (entrywise maximum norm), respectively.

Based on the results in Table 8, in terms of graph selection, joint selection approaches (J.BSSC and J.SSSL) outperform other contenders estimating a graph G without incorporating information about γ . This suggests that joint selection using an MRF prior can benefit not only variable selection performance but also graph selection performance. Furthermore, Table 9 shows that J.BSSC performs significantly better than J.SSSL in terms of precision matrix estimation. In fact, J.BSSC also outperforms the other contenders for all the criteria considered. Therefore, it can be interpreted that joint

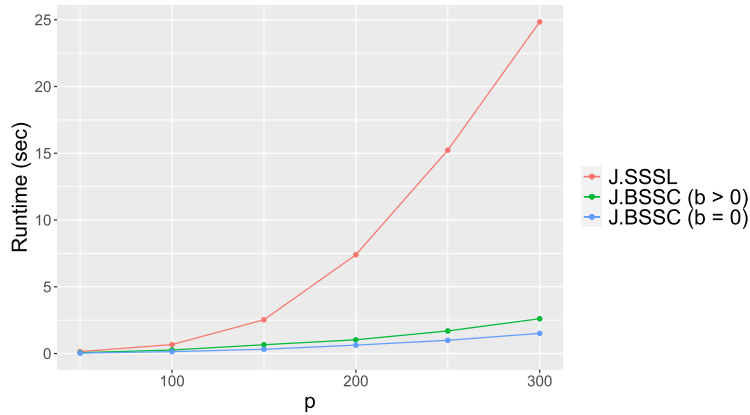


Figure 1: The comparison of average wall-clock seconds per iteration under different dimensions.

selection improves the estimation performance, and in particular, it is more preferable to use CONCORD for precision matrix estimation.

In addition, as noted in Jalali et al. (2020), BSSC is computationally much more efficient compared with SSSL. In Figure 1, we plot the run time comparison between J.BSSC ($b > 0$), J.BSSC ($b = 0$) and J.SSSL under different values of p coded in R. The averaged computation times for J.BSSC are significantly smaller than those for J.SSSL, and the gap between the two gets larger as p grows. Note that with parallel processing, under $b = 0$, one can perform the variable selection and inverse covariance estimation simultaneously, which leads to a relatively lower runtime for J.BSSC ($b = 0$) compared with J.BSSC ($b > 0$). Even in terms of the memory requirement, J.BSSC needs a significantly smaller memory than SSSL. For example, J.SSSL requires more than 20 GB while J.BSSC achieves the goal with 0.22 GB of memory when $p = 300$. Furthermore, based on asymptotic results, one can expect that our method will give accurate inference results as we have more observations, while asymptotic properties of the Bayesian method proposed by Peterson et al. (2016) are still in question.

6 Aberrant Functional Activities in the Parkinson's Disease Cohort

Parkinson's disease (PD) was first described by Dr. James Parkinson in 1817 as "shaking palsy". It is a chronic, progressive neurodegenerative disease characterized by both motor and nonmotor features. As one of the most common neurodegenerative disorders, the disease has a significant clinical impact on patients, families, and caregivers through its progressive degenerative effects on mobility and muscle control. Research suggests that the pathophysiological changes associated with PD may start before the onset of motor features and may include a number of nonmotor presentations, such as sleep disorders,

depression, and cognitive changes. Evidence for this preclinical phase has driven the enthusiasm for research that focuses on early diagnosis and preventive therapies of PD (Schrag et al., 2015).

In recent years, neuroimaging has been increasingly employed to aid the risk stratification in PD. Among a variety of neuroimaging technologies, resting-state fMRI (rs-fMRI) is regarded as a promising technique for precisely locating the abnormal spontaneous activities in neuropsychological disease (Wang et al., 2019). Several rs-fMRI-based methods including regional homogeneity (ReHo), the amplitude of low-frequency fluctuation, and functional connectivity provide a task-free approach to explore spontaneous brain activity and connectivity among networks in different brain regions of PD patients. In this section, we apply the proposed joint selection method to rs-fMRI data for simultaneously identifying aberrant functional brain activities and inferring the underlying functional brain network to aid the diagnosis of PD (Wei et al., 2017; Cao et al., 2020).

6.1 Subjects and Data Preprocessing

This study was approved by the Medical Research Ethical Committee of Nanjing Brain Hospital (Nanjing, China) in accordance with the Declaration of Helsinki, and written informed consent was obtained from all subjects. Seventy PD patients and fifty healthy controls (HCs) were recruited. Image data were acquired using a Siemens 3.0-Tesla signal scanner (Siemens, Verio, Germany) in the department of radiology within Nanjing Brain Hospital. Functional imaging data were collected transversely by using a gradient-recalled echo-planar imaging pulse sequence and retrieved from the archive by neuroradiologists. Image preprocessing steps including slice-timing correction and spatial normalization were carried out using the Data Processing Assistant for Resting-State fMRI based on Statistical Parametric Mapping (SPM12) operated on the Matlab platform (Yan and Zang, 2010).

6.2 Image Feature Extraction

Zang et al. (2004) proposed the method of Regional Homogeneity (ReHo) to analyze characteristics of regional brain activity and to reflect the temporal homogeneity of neural activity. ReHo is defined as a voxel-based measure of brain activity which evaluates the similarity or synchronization between the time series of a given voxel and its nearest neighbors. Abnormal ReHo signals, which are associated with changes in neuronal activity in local brain regions, may be exploited to analyze the abnormal brain activities and to depict the dynamic brain functional connectivities (Xu et al., 2019; Deng et al., 2016). In particular, we focus on the mReHo maps obtained by dividing the mean ReHo of the whole brain within each voxel in the ReHo map. We further segmented the mReHo maps and extracted all the 112 region of interest (ROI) signals based on the Harvard-Oxford atlas (HOA) using the Resting-State fMRI Data Analysis Toolkit (Song et al., 2011).

	Sensitivity	Specificity	MCC	MSPE
J.BSSC ($b > 0$)	0.86	0.86	0.77	0.10
J.BSSC ($b = 0$)	0.67	0.76	0.43	0.18
J.SSSL	0.53	0.78	0.32	0.24
Lasso	0.85	0.75	0.58	0.15
Elastic	0.80	0.75	0.55	0.15

Table 10: The summary statistics for prediction performance on the testing set for all methods.

6.3 Model Fitting

We now consider a probit regression model with the binary disease indicator as an outcome and 112 ReHo radiomic variables as predictors. Various models including the proposed method and other competing approaches will then be implemented to classify subjects based on these extracted features and to learn functional connectivities of the brain. The dataset is randomly divided into a training set (80%) and a testing set (20%) while maintaining the PD:HC ratio in both sets. The hyperparameters for all methods are set as in simulation studies. For Bayesian methods, we first obtain the identified variables and then evaluate the testing set performance using standard GLM estimates based on the selected features. The penalty parameters in all frequentist methods are tuned via 10-fold cross validation in the training set. The final prediction results based on the testing set for both Bayesian and frequentist approaches are evaluated using a common threshold 0.5 and averaged over 10 random splits.

6.4 Results

In this section, we report eight discriminative radiomic features that are most frequently identified among 10 random splits. Specifically, our method is able to consistently identify abnormal functional brain activities for PD that occur in the regions of interest including right superior frontal gyrus (F1.R) (10 times), left middle temporal gyrus, anterior division (T2a.L) (10 times), left angular gyrus (AG.L) (6 times), right angular gyrus (AG.R) (8 times), right temporal fusiform cortex, anterior division (TFa.R) (9 times), right occipital fusiform gyrus (OF.R) (10 times), left frontal operculum cortex (FO.L) (8 times) and left putamen (Put.L) (10 times). It is also worthwhile to mention that similar to the findings in simulation studies, J.BSSC identifies more features connected through the estimated network compared with the separate inference and tends to be more conservative in selecting the regions compared with frequentist approaches. In Figure 2, we plot the inferred functional brain network overlaid with selected nodes that correspond to the aforementioned brain regions. The predictive performance of various methods in the test set is summarized in Table 10. We can tell from Table 10 that the predictive performance of the proposed joint selection approach based on BSSC is overall better than that of all the other methods. The proposed J.BSSC approach has higher sensitivity and lower MSPE compared with all the other methods, but yields a lower specificity than Lasso. Based on the most comprehensive measure MCC, our method outperforms all the other methods.

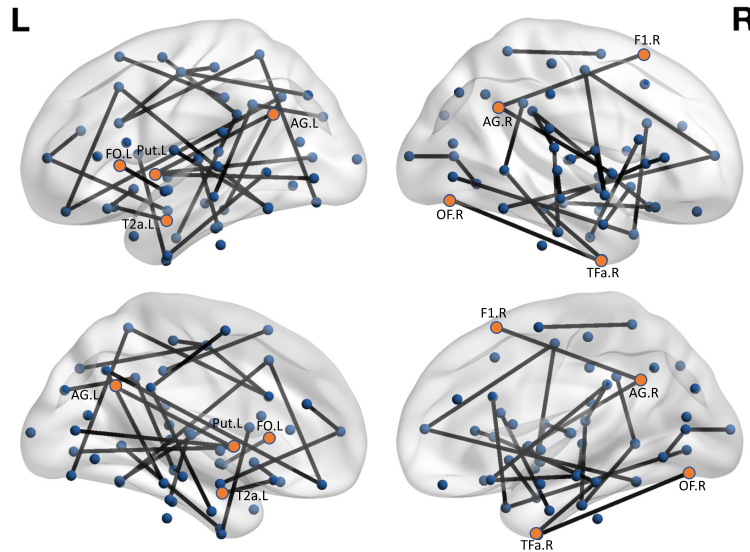


Figure 2: The lateral and medial view of the functional brain network inferred by J.BSSC. Nodes selected by J.BSSC are marked in orange.

Furthermore, J.BSSC identifies regions of interest that are coherent with the altered functional features in cortical and subcortical regions discovered in previous studies (Martin et al., 2009; Zhang et al., 2021; Mihaescu et al., 2019). These findings suggest disease-related alterations of functional activities that provide physicians sufficient information to get involved with early diagnosis and treatment. The inferred functional brain connectivities also seem plausible and are primarily located in the typical resting-state network (RSN) including default-mode network (DMN), visual network (VIN) and basal ganglia network (BGN). The identified regions in DMN include the left middle temporal gyrus, anterior division and angular gyrus. We also discover abnormal VIN in the right temporal fusiform cortex, anterior division and right occipital fusiform gyrus, as well as unusual BGN in the left putamen. RSN reflects the spontaneous neural activities of the blood oxygenation level-dependent signals between temporally correlated brain regions. Compared with the control group, the DMN plays a crucial role in neurodegenerative disorders and normal aging. Several fMRI studies have indicated that the DMN was injured before the cognitive decline in PD (Sandrone and Catani, 2013; Koshimori et al., 2016). The BGN has also been observed in pathologies with motor control and altered neurotransmitter systems of dopaminergic processes (Griffanti et al., 2018; De Micco et al., 2019). A previous study on functional connectivity markers in advanced PD also found functional connectivity features located in the VIN and cerebellar networks that are significantly relevant to classification and provide preliminary evidence that can characterize PD patients compared with HCs (Lin et al., 2020). In conclusion, the radiomics-based joint selection approach proposed in this paper has shown that high-order radiomic features that quantify functional brain connectivities and activities can be used for the diagnosis of PD with satisfactory prediction accuracy.

7 Discussion

We propose a Bayesian joint selection method for probit models. Although it should be rigorously investigated, it is possible to extend the proposed method to other GLMs with network-structured predictors and binary responses. For example, an extension to logistic regression models, in terms of computation, is straightforward by approximating a logistic distribution to mixture of normal distributions (Albert and Chib, 1993; O’Brien and Dunson, 2004). This approximation enables us to derive a similar Gibbs sampler presented in Section 3 with some minor changes; for example, see Lee and Cao (2021a). Furthermore, in theoretical aspect, it is highly expected that joint selection consistency (Theorem 4.4) can be achieved in logistic regression models with CONCORD generalized likelihood by applying the techniques in Lee and Cao (2021a), which efficiently control the score function and Hessian matrix of logistic models.

Theoretical results in this paper, except Theorem 4.1, are based on the conditional posteriors given accurate estimates of diagonal entries, $\hat{\delta}$. This is because we adopt the selection consistency result in Jalali et al. (2020). It would be interesting to investigate whether one can obtain selection consistency without conditioning $\hat{\delta}$ to conduct a fully Bayesian inference. This would need a significant amount of technical modification, so we leave it as future work.

Furthermore, by using CONCORD generalized likelihood, we can enjoy fast computational speed but at the cost of possibly losing the positive definiteness of the precision matrix. Although it does not harm the primary goal of this paper, the selection of the support of the precision matrix and coefficient vector, it will obviously not be satisfactory when the estimation of the precision matrix is of interest. Thus, modifying the CONCORD algorithm to ensure positive definiteness of the precision matrix while maintaining fast computation would be another possible direction of future work.

Supplementary Material

Supplementary to “Consistent and scalable Bayesian joint variable and graph selection for disease diagnosis leveraging functional brain network” (DOI: [10.1214/23-BA1376SUPP](https://doi.org/10.1214/23-BA1376SUPP); .pdf). We present the proofs for the main results and other auxiliary results.

References

- Albert, J. H. and Chib, S. (1993). “Bayesian Analysis of Binary and Polychotomous Response Data.” *Journal of the American Statistical Association*, 88(422): 669–679. [MR1224394](#). 900, 917
- Banerjee, S. and Ghosal, S. (2015). “Bayesian structure learning in graphical models.” *Journal of Multivariate Analysis*, 136: 147–162. [MR3321485](#). doi: <https://doi.org/10.1016/j.jmva.2015.01.015>. 904
- Barbieri, M. M. and Berger, J. O. (2004). “Optimal predictive model selection.” *The*

- Annals of Statistics*, 32(3): 870–897. MR2065192. doi: <https://doi.org/10.1214/009053604000000238>. 907
- Bhadra, A. and Mallick, B. K. (2013). “Joint high-dimensional Bayesian variable and covariance selection with an application to eQTL analysis.” *Biometrics*, 69(2): 447–457. MR3071063. doi: <https://doi.org/10.1111/biom.12021>. 897
- Cai, T., Liu, W., and Luo, X. (2011). “A constrained ℓ_1 minimization approach to sparse precision matrix estimation.” *Journal of the American Statistical Association*, 106(494): 594–607. MR2847973. doi: <https://doi.org/10.1198/jasa.2011.tm10155>. 912
- Cao, X., Khare, K., and Ghosh, M. (2019). “Posterior graph selection and estimation consistency for high-dimensional Bayesian DAG models.” *The Annals of Statistics*, 47(1): 319–348. MR3909935. doi: <https://doi.org/10.1214/18-AOS1689>. 904
- Cao, X. and Lee, K. (2021). “Joint Bayesian variable and DAG selection consistency for high-dimensional regression models with network-structured covariates.” *Statistica Sinica*, 31(3): 1509–1530. MR4297714. doi: <https://doi.org/10.5705/ss.202019.0202>. 897, 904
- Cao, X. and Lee, K. (2023). “Supplementary to “Consistent and scalable Bayesian joint variable and graph selection for disease diagnosis leveraging functional brain network.”” *Bayesian Analysis*. doi: <https://doi.org/10.1214/23-BA1376SUPP>. 897
- Cao, X., Wang, X., Xue, C., Zhang, S., Huang, Q., and Liu, W. (2020). “A Radiomics Approach to Predicting Parkinson’s Disease by Incorporating Whole-Brain Functional Activity and Gray Matter Structure.” *Frontiers in Neuroscience*, 14: 751–751. 914
- Chekouo, T., Stingo, F. C., Doecke, J. D., and Do, K.-A. (2015). “miRNA–target gene regulatory networks: a Bayesian integrative approach to biomarker selection with application to kidney cancer.” *Biometrics*, 71(2): 428–438. MR3366247. doi: <https://doi.org/10.1111/biom.12266>. 897
- Chen, M., Ren, Z., Zhao, H., and Zhou, H. (2016). “Asymptotically normal and efficient estimation of covariate-adjusted Gaussian graphical model.” *Journal of the American Statistical Association*, 111(513): 394–406. MR3494667. doi: <https://doi.org/10.1080/01621459.2015.1010039>. 897
- Consonni, G., La Rocca, L., and Peluso, S. (2017). “Objective Bayes covariate-adjusted sparse graphical model selection.” *Scandinavian Journal of Statistics*, 44(3): 741–764. MR3687971. doi: <https://doi.org/10.1111/sjos.12273>. 897
- De Micco, R., Esposito, F., di Nardo, F., Caiazzo, G., Siciliano, M., Russo, A., Cirillo, M., Tedeschi, G., and Tessitore, A. (2019). “Sex-related pattern of intrinsic brain connectivity in drug-naïve Parkinson’s disease patients.” *Movement Disorders*, 34(7): 997–1005. 916
- Deng, L., Sun, J., Cheng, L., and Tong, S. (2016). “Characterizing dynamic local functional connectivity in the human brain.” *Scientific Reports*, 6(1): 26976. 914
- Deshpande, S. K., Ročková, V., and George, E. I. (2019). “Simultaneous variable and

- covariance selection with the multivariate spike-and-slab lasso." *Journal of Computational and Graphical Statistics*, 28(4): 921–931. MR4045858. doi: <https://doi.org/10.1080/10618600.2019.1593179>. 897
- Dobra, A. (2009). "Variable selection and dependency networks for genomewide data." *Biostatistics*, 10(4): 621–639. 896
- Dobra, A., Lenkoski, A., and Rodriguez, A. (2011). "Bayesian Inference for General Gaussian Graphical Models With Application to Multivariate Lattice Data." *Journal of the American Statistical Association*, 106(496): 1418–1433. MR2896846. doi: <https://doi.org/10.1198/jasa.2011.tm10465>. 896
- Feng, Q., Wang, M., Song, Q., Wu, Z., Jiang, H., Pang, P., Liao, Z., Yu, E., and Ding, Z. (2019). "Correlation Between Hippocampus MRI Radiomic Features and Resting-State Intrahippocampal Functional Connectivity in Alzheimer's Disease." *Frontiers in Neuroscience*, 13: 435. 896
- Friedman, J., Hastie, T., and Tibshirani, R. (2007). "Sparse inverse covariance estimation with the graphical lasso." *Biostatistics*, 9(3): 432–441. 896, 898, 907, 912
- Griffanti, L., Stratmann, P., Rolinski, M., Filippini, N., Zsoldos, E., Mahmood, A., Zamboni, G., Douaud, G., Klein, J. C., Kivimäki, M., Singh-Manoux, A., Hu, M. T., Ebmeier, K. P., and Mackay, C. E. (2018). "Exploring variability in basal ganglia connectivity with functional MRI in healthy aging." *Brain Imaging and Behavior*, 12(6): 1822–1827. 916
- Ishwaran, H., Kogalur, U. B., and Rao, J. S. (2005). "Spike and slab variable selection: Frequentist and Bayesian strategies." *The Annals of Statistics*, 33(2): 730–773. MR2163158. doi: <https://doi.org/10.1214/009053604000001147>. 895
- Jalali, P., Khare, K., and Michailidis, G. (2020). "B-CONCORD – A scalable Bayesian high-dimensional precision matrix estimation procedure." *arXiv preprint arXiv:2005.09017*. 896, 899, 901, 902, 903, 904, 913, 917
- Johnson, V. E. and Rossell, D. (2012). "Bayesian model selection in high-dimensional settings." *Journal of the American Statistical Association*, 107(498): 649–660. MR2980074. doi: <https://doi.org/10.1080/01621459.2012.682536>. 904
- Khare, K., Oh, S.-Y., and Rajaratnam, B. (2015). "A convex pseudolikelihood framework for high dimensional partial correlation estimation with convergence guarantees." *Journal of the Royal Statistical Society: Series B (Statistical Methodology)*, 77(4): 803–825. MR3382598. doi: <https://doi.org/10.1111/rssb.12088>. 896, 897, 898, 905
- Koshimori, Y., Cho, S.-S., Criaud, M., Christopher, L., Jacobs, M., Ghadery, C., Coakley, S., Harris, M., Mizrahi, R., Hamani, C., Lang, A. E., Houle, S., and Strafella, A. P. (2016). "Disrupted Nodal and Hub Organization Account for Brain Network Abnormalities in Parkinson's Disease." *Frontiers in Aging Neuroscience*, 8: 259. 916
- Langer, N., Pedroni, A., Gianotti, L. R., Hänggi, J., Knoch, D., and Jäncke, L. (2012). "Functional brain network efficiency predicts intelligence." *Human Brain Mapping*, 33(6): 1393–1406. 896

- Lee, K. and Cao, X. (2021a). “Bayesian group selection in logistic regression with application to MRI data analysis.” *Biometrics*, 77(2): 391–400. MR4307642. doi: <https://doi.org/10.1111/biom.13290>. 903, 917
- Lee, K. and Cao, X. (2021b). “Bayesian inference for high-dimensional decomposable graphs.” *Electronic Journal of Statistics*, 15(1): 1549–1582. 904
- Li, C. and Li, H. (2008). “Network-constrained regularization and variable selection for analysis of genomic data.” *Bioinformatics*, 24(9): 1175–1182. 896
- Li, C. and Li, H. (2010). “Variable selection and regression analysis for graph-structured covariates with an application to genomics.” *The Annals of Applied Statistics*, 4(3): 1498–1516. MR2758338. doi: <https://doi.org/10.1214/10-AOAS332>. 896
- Li, F. and Zhang, N. R. (2010). “Bayesian Variable Selection in Structured High-Dimensional Covariate Spaces With Applications in Genomics.” *Journal of the American Statistical Association*, 105(491): 1202–1214. MR2752615. doi: <https://doi.org/10.1198/jasa.2010.tm08177>. 900
- Lin, H., Cai, X., Zhang, D., Liu, J., Na, P., and Li, W. (2020). “Functional connectivity markers of depression in advanced Parkinson’s disease.” *NeuroImage: Clinical*, 25: 102130. 916
- Liu, C. and Martin, R. (2019). “An empirical G -Wishart prior for sparse high-dimensional Gaussian graphical models.” *arXiv preprint arXiv:1912.03807*. MR4138128. 904
- Liu, F., Chakraborty, S., Li, F., Liu, Y., and Lozano, A. C. (2014). “Bayesian Regularization via Graph Laplacian.” *Bayesian Analysis*, 9(2): 449–474. MR3217003. doi: <https://doi.org/10.1214/14-BA860>. 896
- Liu, H., Roeder, K., and Wasserman, L. (2010). “Stability Approach to Regularization Selection (StARS) for High Dimensional Graphical Models.” In *Proceedings of the 23rd International Conference on Neural Information Processing Systems – Volume 2*, NIPS’10, 1432–1440. 912
- Liu, H. and Wang, L. (2017). “TIGER: A tuning-insensitive approach for optimally estimating Gaussian graphical models.” *Electronic Journal of Statistics*, 11(1): 241–294. MR3606771. doi: <https://doi.org/10.1214/16-EJS1195>. 912
- Martin, R., Mess, R., and Walker, S. G. (2017). “Empirical Bayes posterior concentration in sparse high-dimensional linear models.” *Bernoulli*, 23(3): 1822–1847. MR3624879. doi: <https://doi.org/10.3150/15-BEJ797>. 904
- Martin, W. W., Wieler, M., Gee, M., and Camicioli, R. (2009). “Temporal lobe changes in early, untreated Parkinson’s disease.” *Movement Disorders*, 24(13): 1949–1954. 916
- Meinshausen, N. and Bühlmann, P. (2006). “High-dimensional graphs and variable selection with the lasso.” *The Annals of Statistics*, 34(3): 1436–1462. MR2278363. doi: <https://doi.org/10.1214/009053606000000281>. 896, 898, 910

- Mihaescu, A. S., Masellis, M., Graff-Guerrero, A., Kim, J., Criaud, M., Cho, S. S., Ghadery, C., Valli, M., and Strafella, A. P. (2019). “Brain degeneration in Parkinson’s disease patients with cognitive decline: a coordinate-based meta-analysis.” *Brain Imaging and Behavior*, 13(4): 1021–1034. 916
- Nacu, Ș., Critchley-Thorne, R., Lee, P., and Holmes, S. (2007). “Gene expression network analysis and applications to immunology.” *Bioinformatics*, 23(7): 850–858. 896
- Narisetty, N. N. and He, X. (2014). “Bayesian variable selection with shrinking and diffusing priors.” *The Annals of Statistics*, 42(2): 789–817. MR3210987. doi: <https://doi.org/10.1214/14-AOS1207>. 895, 900, 903, 904
- Narisetty, N. N., Shen, J., and He, X. (2019). “Skinny Gibbs: A Consistent and Scalable Gibbs Sampler for Model Selection.” *Journal of the American Statistical Association*, 114(527): 1205–1217. MR4011773. doi: <https://doi.org/10.1080/01621459.2018.1482754>. 904
- O’Brien, S. M. and Dunson, D. B. (2004). “Bayesian multivariate logistic regression.” *Biometrics*, 60(3): 739–746. MR2089450. doi: <https://doi.org/10.1111/j.0006-341X.2004.00224.x>. 917
- Park, T. and Casella, G. (2008). “The Bayesian Lasso.” *Journal of the American Statistical Association*, 103(482): 681–686. MR2524001. doi: <https://doi.org/10.1198/016214508000000337>. 901
- Peluso, S. and Consonni, G. (2020). “Compatible priors for model selection of high-dimensional Gaussian DAGs.” *Electronic Journal of Statistics*, 14(2): 4110–4132. MR4170698. doi: <https://doi.org/10.1214/20-EJS1768>. 897
- Peng, J., Wang, P., Zhou, N., and Zhu, J. (2009). “Partial Correlation Estimation by Joint Sparse Regression Models.” *Journal of the American Statistical Association*, 104(486): 735–746. MR2541591. doi: <https://doi.org/10.1198/jasa.2009.0126>. 896, 905
- Peterson, C. B., Stingo, F. C., and Vannucci, M. (2016). “Joint Bayesian variable and graph selection for regression models with network-structured predictors.” *Statistics in Medicine*, 35(7): 1017–1031. MR3476525. doi: <https://doi.org/10.1002/sim.6792>. 897, 900, 907, 912, 913
- Ročková, V. and George, E. I. (2018). “The spike-and-slab lasso.” *Journal of the American Statistical Association*, 113(521): 431–444. MR3803476. doi: <https://doi.org/10.1080/01621459.2016.1260469>. 895
- Salvatore, C., Castiglioni, I., and Cerasa, A. (2021). “Radiomics approach in the neurodegenerative brain.” *Aging Clinical and Experimental Research*, 33(6): 1709–1711. 896
- Samanta, S., Khare, K., and Michailidis, G. (2022). “A generalized likelihood-based Bayesian approach for scalable joint regression and covariance selection in high dimensions.” *Statistics and Computing*, 32(3): 1–23. MR4434166. doi: <https://doi.org/10.1007/s11222-022-10102-5>. 897

- Sandrone, S. and Catani, M. (2013). “Journal Club: Default-mode network connectivity in cognitively unimpaired patients with Parkinson disease.” *Neurology*, 81(23): e172–e175. [916](#)
- Schrag, A., Horsfall, L., Walters, K., Noyce, A., and Petersen, I. (2015). “Prediagnostic presentations of Parkinson’s disease in primary care: a case-control study.” *The Lancet Neurology*, 14(1): 57–64. [914](#)
- Song, X.-W., Dong, Z.-Y., Long, X.-Y., Li, S.-F., Zuo, X.-N., Zhu, C.-Z., He, Y., Yan, C.-G., and Zang, Y.-F. (2011). “REST: A Toolkit for Resting-State Functional Magnetic Resonance Imaging Data Processing.” *PLOS ONE*, 6(9): 1–12. [914](#)
- Souza, L. P. D., Alseekh, S., Brotman, Y., and Fernie, A. R. (2020). “Network-based strategies in metabolomics data analysis and interpretation: from molecular networking to biological interpretation.” *Expert Review of Proteomics*, 17(4): 243–255. [896](#)
- Stingo, F. C. and Vannucci, M. (2010). “Variable selection for discriminant analysis with Markov random field priors for the analysis of microarray data.” *Bioinformatics*, 27(4): 495–501. [900](#)
- Tibshirani, R. (1996). “Regression shrinkage and selection via the lasso.” *Journal of the Royal Statistical Society: Series B (Methodological)*, 58(1): 267–288. [MR1379242](#). [895](#), [907](#)
- Wainwright, M. J. (2019). *High-Dimensional Statistics: A Non-Asymptotic Viewpoint*. Cambridge Series in Statistical and Probabilistic Mathematics. Cambridge University Press. [MR3967104](#). doi: <https://doi.org/10.1017/9781108627771>. [896](#)
- Wang, H. (2012). “Bayesian Graphical Lasso Models and Efficient Posterior Computation.” *Bayesian Analysis*, 7(4): 867 – 886. [MR3000017](#). doi: <https://doi.org/10.1214/12-BA729>. [896](#), [898](#)
- Wang, H. (2015). “Scaling it up: Stochastic search structure learning in graphical models.” *Bayesian Analysis*, 10(2): 351–377. [MR3420886](#). doi: <https://doi.org/10.1214/14-BA916>. [896](#), [899](#), [900](#), [907](#), [912](#)
- Wang, Y., Sun, K., Liu, Z., Chen, G., Jia, Y., Zhong, S., Pan, J., Huang, L., and Tian, J. (2019). “Classification of Unmedicated Bipolar Disorder Using Whole-Brain Functional Activity and Connectivity: A Radiomics Analysis.” *Cerebral Cortex*, 30(3): 1117–1128. [914](#)
- Wei, L., Hu, X., Zhu, Y., Yuan, Y., Liu, W., and Chen, H. (2017). “Aberrant intra- and internetwork functional connectivity in depressed Parkinson’s disease.” *Scientific Reports*, 7(1): 1–12. [914](#)
- Xiang, R., Khare, K., and Ghosh, M. (2015). “High dimensional posterior convergence rates for decomposable graphical models.” *Electronic Journal of Statistics*, 9(2): 2828–2854. [MR3439186](#). doi: <https://doi.org/10.1214/15-EJS1084>. [904](#)
- Xu, X. and Ghosh, M. (2015). “Bayesian Variable Selection and Estimation for Group Lasso.” *Bayesian Analysis*, 10(4): 909–936. [MR3432244](#). doi: <https://doi.org/10.1214/14-BA929>. [902](#)

- Xu, Z., Lai, J., Zhang, H., Ng, C. H., Zhang, P., Xu, D., and Hu, S. (2019). “Regional homogeneity and functional connectivity analysis of resting-state magnetic resonance in patients with bipolar II disorder.” *Medicine*, 98(47). 914
- Yan, C. and Zang, Y. (2010). “DPARSF: a MATLAB toolbox for “pipeline” data analysis of resting-state fMRI.” *Frontiers in Systems Neuroscience*, 4: 13. 914
- Yang, X. and Narisetty, N. N. (2020). “Consistent Group Selection with Bayesian High Dimensional Modeling.” *Bayesian Analysis*, 15(3): 909–935. MR4132654. doi: <https://doi.org/10.1214/19-BA1178>. 902
- Yang, Y., Wainwright, M. J., and Jordan, M. I. (2016). “On the computational complexity of high-dimensional Bayesian variable selection.” *The Annals of Statistics*, 44(6): 2497–2532. MR3576552. doi: <https://doi.org/10.1214/15-AOS1417>. 900
- Yuan, M. and Lin, Y. (2007). “Model selection and estimation in the Gaussian graphical model.” *Biometrika*, 94(1): 19–35. MR2367824. doi: <https://doi.org/10.1093/biomet/asm018>. 896, 898
- Zang, Y., Jiang, T., Lu, Y., He, Y., and Tian, L. (2004). “Regional homogeneity approach to fMRI data analysis.” *NeuroImage*, 22(1): 394–400. 914
- Zhang, X., Cao, X., Xue, C., Zheng, J., Zhang, S., Huang, Q., and Liu, W. (2021). “Aberrant functional connectivity and activity in Parkinson’s disease and comorbidity with depression based on radiomic analysis.” *Brain and Behavior*, 11(5): e02103. 916
- Zou, H. and Hastie, T. (2005). “Regularization and variable selection via the elastic net.” *Journal of the Royal Statistical Society: Series B (Statistical Methodology)*, 67(2): 301–320. MR2137327. doi: <https://doi.org/10.1111/j.1467-9868.2005.00503.x>. 907

Acknowledgments

We are grateful to the Editor, Associate Editor and reviewers for their valuable comments which have significantly improved the quality of presentation and technical content of our paper.